Parameter optimization and test based on discrete element method for biaxial layered cutting and deep rotary tillage process in rice stubble fields

Yifu Zhang[1,2], Wen Shi[1], Huini Zhou[3*], Xiaogang Zheng[4]

(1. *School of Mechanical Engineering, Yangzhou University, Yangzhou 225127, Jiangsu, China*;
2. *Vegetable (Root vegetable) Fully Mechanized Research Base, Ministry of Agriculture and Rural Affairs, Yangzhou 225009, China*;
3. *Business School, Yangzhou University, Yangzhou 225127, Jiangsu, China*;
4. *Jiangsu Agricultural Mechanization Service Station, Nanjing 210017, Jiangsu, China*)

Abstract: Straw incorporation into farmlands is recognized as beneficial for improving cultivated land quality, stimulating soil carbon sinks, and promoting crop growth. However, in the rice-wheat double-cropping system, the postharvest period results in abundant crop straw, leading to prominent straw surplus issues. Problems such as the tight schedule between harvesting and sowing and high-quality requirements for seedbeds result in traditional rotary tillage, which often results in excess straw in the tillage layer and straw piles, severely restricting sowing quality. To address these issues, a technological solution was proposed involving biaxial layered cutting for deep rotary tillage and uniform mixing of straw. The focus was on the biaxial deep rotary tillage and uniform mixing processes, along with device testing in paddy fields, via the discrete element method. A composite discrete element model of root stubble, soil, and rice straw was established for a typical rice-wheat rotation area in Jiangsu Province, China, and coupled with a biaxial rotary tillage unit. Using the response surface analysis method, the vertical height difference of the rear cutter shaft relative to the front cutter shaft (L_n), the rotation speed of the cutter group (w), and the forwards speed of the unit (v) were considered the three factors affecting rotary tillage quality. A three-factor, three-level orthogonal simulation test was conducted, yielding the optimal parameter combination: L_n = –73.3 mm, w = 273.6 r/min, and v = 0.6 m/s. Under this combination, the tillage performance achieved a total power consumption of 29.66 kW and a straw burial rate of 94.6%. The results of the prototype field test indicated that the biaxial rotary tillage device significantly loosened the top 20 cm of the soil layer, with a post-tillage surface flatness of 2.80 cm, a straw burial rate of 92.6%, and a tillage depth stability of 95.3%, meeting the quality requirements for the incorporation of straw rotary tillage. The results of this study can provide a theoretical basis and case reference for achieving high-quality mechanized straw incorporation in rice-wheat rotation systems.

Keywords: straw returning, discrete element method, biaxial deep rotary tillage, parameter optimization
DOI: 10.25165/j.ijabe.20251805.9300

Citation: Zhang Y F, Shi W, Zhou H N, Zheng X G. Parameter optimization and test based on discrete element method for biaxial layered cutting and deep rotary tillage process in rice stubble fields. Int J Agric & Biol Eng, 2025; 18(5): 171–180.

1 Introduction

Straw returning refers to the incorporation of straw produced during crop production into farmland[1]. This measure is advantageous for improving soil fertility and increasing crop yield by 5%-10% while eliminating the air pollution caused by straw burning[2-4]. Specifically, many studies have indicated its advantages in improving physicochemical properties[5], and promoting microbial activity[6] and crop root development[7,8], which is beneficial for improving cultivated land quality on a global scale.

Jiangsu is a crucial grain-producing region in the mid-lower reaches of the Yangtze River in China that primarily practices a double cropping system of rice and wheat. This multi-cropping production mode results in a substantial amount of crop straw each planting season, with rice straw excess being particularly prominent[9]. Especially in this region, the clay-heavy soil texture and greater tillage resistance significantly increase the difficulty of straw incorporation operations and agricultural production costs. Traditional rotary tillers, due to their shallow working depth, tend to cause problems such as excessive straw ratio in the tillage layer, straw clumping, and uneven distribution of straw residues. This impedes root development and, if improperly managed, can also lead to increased soil pathogens, aggravated crop diseases, and even reduced yields along with issues like poor seedling emergence and stunted seedlings. Therefore, appropriate straw-returning measures and equipment must be implemented to achieve seedbed qualities that meet agronomic standards.

Mechanizing straw return directly into stubble fields postharvest is an effective approach to reduce labor intensity and increase work efficiency. Current research on straw-returning equipment focuses primarily on optimizing blade structural parameters, innovating machinery, and developing rotary tillage and burial theories[10-14]. Curved blades, as the primary model of rotary tiller blades, have sharp edges that achieve excellent shearing effects during tillage, facilitating the cutting of stems and the breaking of soil[15,16]. Shi et al.[17] conducted a comprehensive analysis of rotary tiller blade parameters, such as the external opening angle, sliding pushing angle, and blade quantity, to improve the quality of seedbed preparation. In recent years, more scholars have concentrated on designs that reduce resistance and enhance efficiency, upgrade components, and integrate multifunctional features. For example, Yuan et al.[18] analyzed the tillage resistance

Received date: 2024-08-16 **Accepted date:** 2025-07-07
Biographies: Yifu Zhang, Associate Professor, research interest: conservation agriculture, agriculture machine and equipment engineering, Email: zyfu@yzu.edu.cn; **Wen Shi**, MS, research interest: agricultural equipment, Email: 932343708@qq.com; **Xiaogang Zheng**, Professorate Senior Engineer, research interest: agricultural equipment, Email: 13851886389@163.com.
***Corresponding author: Huini Zhou**, Associate Professor, research interest: agricultural supply chain. Business School, Yangzhou University, No. 196, Huayangxilu, Hanjiang District, Yangzhou 225127, Jiangsu, China. Tel: +86-514-87991909, Email: 779807350@qq.com.

components of rotary blades and their relationships with operating parameters and developed a mathematical relationship between tillage resistance and energy consumption. Xiao et al.[19] improved the stability of tillage depth based on the fuzzy proportional integral derivative (PID) control method. Liu et al.[20] developed an intelligent vibration detachment system to solve the adhesion and winding problem of the roller with the soil and straw stubble. Du et al.[21] and Zheng et al.[22] designed a combined tillage implementation by optimizing anti-vibrating and anti-wrapping rotary components, which improved stubble wrapping and returning quality.

A review of the literature reveals that the complex and variable nature of farmland soil environments makes it challenging to study the operating processes and mechanisms of rotary tillage devices. The discrete element method (DEM) is a particle-based analysis method grounded in molecular dynamics principles that views the research object as a collection of discrete particles[23,24]. DEM establishes mathematical models based on the physical properties of materials, mechanics, and Newton's laws of motion, and they have garnered extensive attention in the fields of soil mechanics and agricultural machinery[25]. For instance, Walton et al.[26] created a hysteretic spring model (HSM) to characterize the plastic deformation of materials for plastic material deformation issues. Ucgul et al.[27] combined the HSM and the linear cohesion model to represent the plastic deformation and cohesion of soil, addressing the plastic deformation problem of cohesive soils. Zhang et al.[28] developed a soil particle bonding model tailored to the characteristics of sandy silty soils, which are low in cohesion, large, and loose, aiding in understanding the energy consumption characteristics of rotary tillage cutting. In recent years, Chen et al.[29] established a soil-straw composite model using the DEM for undisturbed soil under straw coverage conditions, which can accurately predict the mechanical behavior of soil contact components. Using multi-body dynamics (MBD)-DEM coupling method, Wang et al.[30] and Lin et al.[31] carried out a simulation experiment on the ditching and returning device for the rice straw and an exploration of straw movement through machine-straw-soil interaction simulation, respectively. Zhu et al.[32] and Zhang et al.[33] employed a DEM to establish a coupled simulation system of tools, straw, and soil, further analyzing the rotary tillage process in rice-wheat rotation systems.

Straw mixing is a crucial technical approach to increase the soil carbon sequestration potential, with the burial rate and uniform distribution of residues in the soil layer being key to ensuring tillage and seeding quality[34,35]. Notably, tillage depth is the primary factor influencing the effectiveness of straw burial[36-38]. The overall trend indicates that improving straw incorporation quality requires balance between increasing stubble breaking and tillage depth to reduce the straw proportion in the tillage layer and using double-shaft cutting to promote the uniform distribution of straw within the soil layer. However, research on soil-straw deep tillage mixtures is scarce. Specifically, the issue of ensuring straw burial effectiveness and distribution uniformity in environments with high straw return volumes on stubble fields remains unresolved. Currently, research on the adjustment of tillage blade configurations and operational parameters remains predominantly limited to single-axis rotary tillage scenarios. Studies investigating the deepening mechanisms during dual-axis rotary tillage processes and their effects on straw burial performance remain scarce.

To address the regional challenges of clay-heavy soil texture, substantial rice straw incorporation, and tightly scheduled cultivation and planting cycles in the rice-wheat rotation systems of China's middle-lower Yangtze River region, a deep rotary tillage solution for straw incorporation was proposed based on the dual-axis layered cutting mechanism. A stubble-soil-rice straw composite model was constructed based on the DEM, a tillage simulation system for rice stubble field environments was established, and the movement characteristics of straw during double-axis rotary tillage processes were analyzed. Additionally, response surface methodology is employed to design and optimize a set of tillage parameters that achieve optimal rotary tillage quality, and the tillage effects are verified through prototype testing. The objectives of the study were (1) to design a biaxial deep rotary tillage device based on a layered cutting scheme and (2) to determine the optimal operational parameters for double-axis rotary tillage to achieve the best straw return quality, and therefore to provide a theoretical foundation and case reference for achieving high-quality mechanized straw incorporation in the rice-wheat rotation systems throughout the mid-lower region of Yangtze River in China.

2 Root stubble-soil-rice straw composite model based on DEM

2.1 Soil model

A simulation system for the root stubble-soil-rice straw composite model was established based on the DEM. To ensure computational efficiency, the soil particle diameter was set to 20 mm. The soil particles were generated randomly in the particle factory, with particle sizes ranging from 0.8 to 1.2 times the original particle size. The rice-wheat rotation system in the mid-lower reaches of Yangtze River leads to year-round alternating dry-wet conditions in the soil, which is generally of a clay texture. The Hertz-Mindlin with bonding particle contact model can simultaneously reflect the soil's discontinuity and agglomeration characteristics, effectively addressing the nonlinear issues of the interaction between agricultural tools and soil. This model aligns well with the mechanical behavior characteristics of wet clayey soil after rice stubble crushing. Therefore, the Hertz-Mindlin with bonding model was employed to represent the bonding characteristics between the soil particles (Figure 1). Soil samples were collected in Jiangyan District (120°07′E, 32°36′N), Taizhou City, Jiangsu Province, which is a typical double-cropping rice-wheat rotation region. Relevant parameters were tested using a 100 cm^3 cutting ring sampler, the oven-drying method, and triaxial tests. The soil model is divided into two layers. The soil particle density, Poisson's ratio, and shear modulus of the upper plough layer were set to 2400 kg/m^3, 0.3, and 1.0 MPa, respectively, and those of the plow pan were 2680 kg/m^3, 0.3, and 1.0 MPa, respectively. The main contact parameters for the soil particles were obtained from the literature[39,40] (Table 1), in which the soil characteristics or farming systems were close to those in this study.

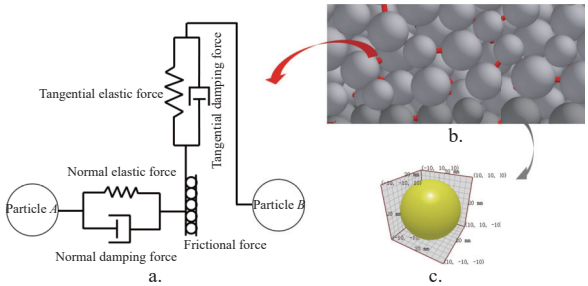

Figure 1 Soil particle contact model based on discrete element method with (a) contact model, (b) schematic diagram of bond model between soil particles, and (c) soil particle model

Table 1 Soil model contact parameter setting

Parameters	Values
Recovery coefficient within plough layer	0.4
Static friction coefficient within plough layer	0.3
Rolling friction coefficient within plough layer	0.1
Recovery coefficient within plow pan	0.4
Static friction coefficient within plow pan	0.35
Rolling friction coefficient within plow pan	0.18
Recovery coefficient between plough layer and plow pan	0.32
Static friction coefficient between plough layer and plow pan	0.6
Rolling friction coefficient between plough layer and plow pan	0.3

2.2 Rice root stubble model

The simplified rice root stubble model was constructed using SolidWorks. Spherical particle splicing was then applied in EDEM 2021 to locate all the particle coordinates for rapid root system modeling, as depicted in Figure 2. During model construction, the number of particles for a single root system was set to 2943 to closely approximate the actual root shape. This study focused on analyzing the movement characteristics of root stubble within the soil environment, and root breakage and fragmentation were not considered to improve simulation efficiency. Other related parameters are presented in Table 2.

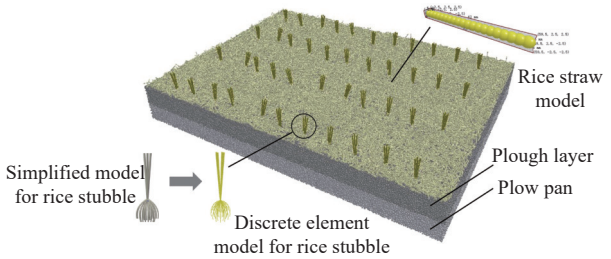

Figure 2 Schematic diagram of rice stubble-soil-straw discrete element composite model

Table 2 Parameter setting for rice root stubble model

Parameters	Values
Per rice root stubble particle number	2943
Particle radius/mm	1.3
Particle density/g·cm^{-3}	0.12
Shear modulus/MPa	6.3

2.3 Rice straw model

The rice straw model was constructed using particle splicing (Figure 2). Before modeling, the 3D dimensions of the rice straw fragments were measured and simplified. The simplified model consisted of 21 spheres, each with a radius of 2.5 mm, arranged to form a total length of 59 mm. Like the root stubble model, the straw model was set as a rigid unit that would not be cut. The Hertz-Mindlin no-slip contact model was used to describe the contact characteristics of the straw particles, with other parameters detailed in Table 3[41,42].

The designed root-soil-rice straw discrete element composite model is shown in Figure 2. The soil trough was 4000 mm long and 1000 mm wide. The soil layer was divided into two layers: the upper plough layer, with a thickness of 120 mm, and the lower plow pan, with a thickness of 100 mm. The stable operating path of the machine was concentrated in the middle of the soil trough. Therefore, straw and root stubble were generated only in the 1000 mm×3000 mm area in the center of the soil trough to increase the simulation efficiency. In accordance with agronomic row spacing standards, the number of generated root stubbles was set to 36.

Table 3 Parameter setting of rice straw particle model

Parameters	Values
Rice straw particle density/g·cm^{-3}	0.241
Poisson's ratio	0.4
Shear modulus/MPa	1.0
Recovery coefficient between rice straw	0.3
Static friction coefficient between rice straw	0.3
Rolling friction coefficient between rice straw	0.01

3 Simulation system for biaxial deep rotary tillage and soil-straw mixing

3.1 Biaxial rotary tillage components and the layered cutting principle

Figure 3a shows the biaxial rotary tillage device designed in this study. It is primarily composed of a suspension frame, a side transmission box, an intermediate speed change gearbox, front and rear rotary tillage blade assemblies, and a rear leveling board. The device is connected to a tractor using a three-point suspension system and linked to the rear power output shaft of the tractor via a universal joint drive shaft. The transmission box in the middle of the device is also connected to the side transmission gearboxes of the front and rear blade shafts through universal joint drive shafts, enabling power transmission. The front and rear rotary tillage blade assemblies perform soil tillage and stubble removal, whereas the rear leveling board levels the soil surface.

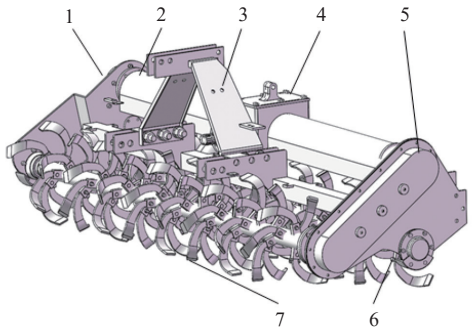

a.

1.Side-rear transmission gearbox 2.Transmission shaft 3.Three-point suspension 4.Intermediate transmission gear box 5.Side front transmission gearbox 6.Backward rotary blade group 7.Forward rotary blade group

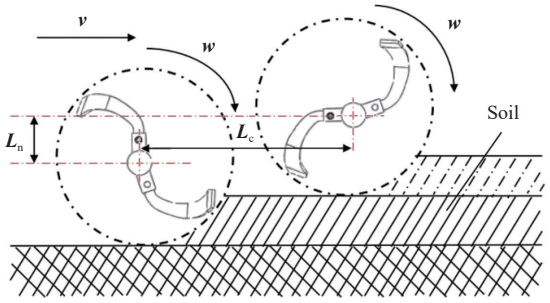

b.

Note: L_n is the vertical height of the rear cutter shaft relative to the front cutter shaft, mm; L_c is the horizontal distance of the rear cutter shaft relative to the front cutter shaft, mm; v is forwards speed of the unit, m/s; w is rotation speed of the cutter group, r/min.

Figure 3 Schematic diagram of (a) biaxial rotary tillage component model and (b) layered cutting arrangement for biaxial rotary tillage axes

Importantly, the biaxial rotary tillage components exhibit a stepped spatial arrangement (Figure 3b). Specifically, the first rotary tillage blade shaft is positioned above and in front of the second blade shaft; the first blade shaft is located at the top and the second blade shaft at the bottom; and the first blade shaft is at the front and the second blade shaft at the rear. The tillage area of the blades on the front shaft overlaps with that of the blades on the rear shaft, ensuring that the rear blades can penetrate the soil effectively. During operation, the first blade shaft initially tills the soil layer to a depth of 10-15 cm. Following this initial tillage, the second blade shaft performs an additional deep tillage of 10-15 cm, ensuring that the total tillage depth exceeds 20 cm.

3.2 Construction of the biaxial rotary tillage system

The biaxial deep rotary tillage system for rice stubble fields, which is based on the DEM, is shown in Figure 4. It was developed by coupling the root-soil-straw composite DEM model with the biaxial rotary tillage device using EDEM 2021 software. The number of generated straw particles is set to 20 650 based on bulk density. The forwards speed of the simulation unit is set to 0.6 m/s, with both front and rear rotary tillage blade shafts rotating forward at a speed of 270 r/min. The tillage depth is set to 210 mm. The relevant parameters of the tillage model are summarized in Table 4.

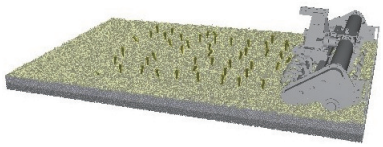

Figure 4 Biaxial deep rotary tillage system for rice stubble fields based on the DEM

Table 4 Setting of related parameters for rotary tillage simulation model

Parameters	Values
Density of tillage components/g·cm^{-3}	7.865
Poisson's ratio of tillage components	0.3
Shear modulus of tillage components/MPa	7.9×10^4
Recovery coefficient between soil and tillage components	0.6
Static friction coefficient between soil and tillage components	0.6
Rolling friction coefficient between soil and tillage components	0.05
Recovery coefficient between straw and tillage components	0.3
Static friction coefficient between straw and tillage components	0.3
Rolling friction coefficient between straw and tillage components	0.01
Recovery coefficient between root stubble and tillage components	0.3
Static friction coefficient between root stubble and tillage components	0.3
Rolling friction coefficient between root stubble and tillage components	0.01
Recovery coefficient between soil and straw	0.5
Static friction coefficient between soil and straw	0.5
Rolling friction coefficient between soil and straw	0.05
Recovery coefficient between soil and root stubble	0.5
Static friction coefficient between soil and root stubble	0.5
Rolling friction coefficient between soil and root stubble	0.05

The efficiency of DEM simulations correlates with the complexity of the device. To increase the efficiency of the simulation system, the rotary tillage unit is simplified equivalently. The simplified model uses front and rear rotary blade shafts, each 0.9 m long, excluding bolts, bearings, and other components that do not affect the simulation results. It retains only the top cover, rear leveling board, and left and right side panels. The unit's cover has a single linear motion, added directly as "Linear Translation." The blade assembly motion includes both linear and rotational movements, with the blade shaft centroid directly adding linear motion ("Linear Translation") and forwards rotation ("Linear Rotation"). The time step is set to 0.2, the simulation time is set to 8 s, and the mesh element size is set to 9 times the minimum particle radius. The tillage simulation process of the simplified unit is shown in Figure 5.

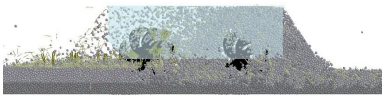

Figure 5 Discrete element simulation process for biaxial deep rotary tillage system

3.3 Simulation metrics and methods

3.3.1 Power consumption

The total power consumption of the machine is calculated by summing the power consumption of the front and rear rotary tillage blade assemblies during operation. In the simulation environment, the rotational speed of the machine is set as a constant value. It is necessary to collect the torque characteristics of the front and rear blade shafts during the simulation. The post-processing module is used to gather torque data. In the Create Graph tab, the *X*-axis is set to time (1.8-3.8 s), and the *Y*-axis is set to total torque (Total-Torque). This step generates a graph depicting the relationship between the torque of the rotary tillage components and time over a period of 2 s.

3.3.2 Straw burial rate

The straw burial rate refers to the percentage of straw incorporated into the soil after tillage, relative to the total straw weight before the operation. In accordance with the quality standards for rotary tillage operations, straw burial rate is defined as the ratio of the mass of straw buried in the soil after rotary tillage to the mass of straw present on the surface before tillage at the same measurement point. Using the 3D viewer tab in the post-processing module, a new grid bin group is created in the setup selections module to select straw particles. The size of the collection domain is set to 500 mm×500 mm×200 mm. The collection depth was adjusted according to the actual tillage conditions to ensure that all straw below the surface was captured. The burial rate is calculated after data collection. The collection and distribution of straw data before and after rotary tillage are illustrated in Figure 6.

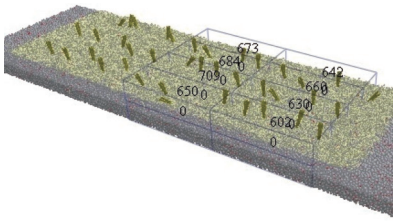

a. Straw data collection before rotational tillage

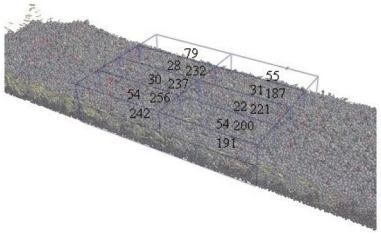

b. Straw data collection after rotational tillage

Figure 6 Schematic diagram of total straw data collection and distribution

3.3.3 Field surface flatness after tillage

Soil surface flatness after tillage is defined as the coefficient of variation in micro-topographic elevation, indicating the ability of tillage machinery to homogenize the soil. After the biaxial rotary tillage simulation, the surface flatness is analyzed using the post-processing mesh division function. Once the particles are stabilized following the operation, the selection function in the post-processing module is used to add a mesh. The soil trough cross-section is selected for flatness analysis.

4 Parameter optimization based on response surface methodology

The author initially conducted a single-factor simulation study on the impact of different tillage parameters on the quality of rotary tillage. The results indicated that tillage parameters had a minimal effect on the surface flatness of the soil after tillage. However, the vertical distance of the rear shaft relative to the front shaft (L_n), the rotational speed of the front and rear blade shafts (w), and the forwards speed of the front and rear blade shafts (v) are key structural and operational parameters affecting the power consumption and straw burial rate during rotary tillage (not shown in this study). Therefore, this study employed the response surface Box-Behnken design to conduct an experimental design and used the biaxial rotary tillage simulation model to perform a three-factor simulation test of tillage quality. The aim was to analyze the influence of the aforementioned three key parameters on the performance of biaxial rotary tillage and obtain the optimal parameter combination for achieving the best tillage performance.

4.1 Experimental design

Response surface optimization was adopted, with the vertical distance of the rear shaft relative to the front shaft (L_n), the rotational speed of the blade shaft (w), and the machine's forwards speed (v) designed as the parameters to be optimized. The power consumption PC and straw burial rate M were used as test indicators. The Box-Behnken method was utilized in Design Expert software for experimental design. Table 5 lists the levels of the test parameters.

Table 5 Level coding table for test factors

Level	Factors		
	L_n/mm	w/r·min^{-1}	v/m·s^{-1}
–1	0	240	0.6
0	–40	270	0.9
1	–80	300	1.2

Note: L_n is the vertical distance of the rear shaft relative to the front shaft, mm; w is the rotational speed of the blade shaft, r/min; and v is the machine's forwards speed, m/s. The same as below.

4.2 Analysis of results

4.2.1 Influence of tillage parameters on power consumption

The influence of the tillage parameters on the power consumption results of the biaxial rotary tillage simulation tests is shown in Table 6. Multiple regression fitting was conducted on the simulation test results. Table 7 presents the analysis of variance (ANOVA) for the power consumption simulation test results, validating the effectiveness of the power consumption fitting equation. According to Table 7, the F-value of the quadratic model for the power consumption response surface is 183.35 (p<0.0001), indicating that the model is highly significant. The lack-of-fit term is 0.2099 and greater than 0.05, indicating that the lack of fit is not significant. This result suggests that the quadratic model for the power consumption response surface has a good fit with minimal error interference, making it suitable for replacing actual test points when analyzing the relationships between power consumption and various parameters. For the regression model of power consumption P, the regression terms L_n, w, v, $L_n{\cdot}v$, $w{\cdot}v$, and L_n^2 have highly significant impacts.

Table 6 Influence of tillage parameters on the power consumption in the biaxial deep rotary tillage simulation

Serial number	L_n/mm	w/r·min^{-1}	v/m·s^{-1}	PC/kW
1	0	0	0	15.6
2	–1	0	–1	10.78
3	1	0	1	21.93
4	0	–1	1	15.79
5	–1	1	0	15.96
6	0	–1	–1	11.59
7	1	1	0	22.26
8	0	1	–1	14.68
9	0	1	1	20.41
10	0	0	0	15.6
11	1	0	–1	19.94
12	–1	–1	0	11.73
13	–1	0	1	17.34
14	0	0	0	15.58
15	1	–1	0	19.11

Note: PC is power consumption, kW.

Table 7 Variance analysis results of power consumption response surface model

Source	Quadratic sum	Freedom	Mean square	F-value	p-value
Model	161.88	6	26.98	183.35	< 0.0001**
L_n	75.58	1	75.58	513.63	< 0.0001**
w	22.01	1	22.01	149.58	< 0.0001**
v	51.11	1	51.11	347.29	<0.0001**
$L_n{\cdot}v$	2.39	1	2.39	16.22	0.0024**
$w{\cdot}v$	2.45	1	2.45	16.64	0.0022**
L_n^2	8.35	1	8.35	56.71	< 0.0001**
Residual error	1.47	10	0.1472		
Lack of fit	1.26	6	0.2099	3.96	0.1019
Pure error	0.212	4	0.053		
Summation	163.35	16			

Note: ** indicates highly significant (p<0.01).

Insignificant terms were removed from the model, retaining the coefficients of significant terms. The regression equation for power consumption (PC) was refitted, ensuring a highly significant fit. The optimized regression equation is as follows:

$$PC = 15.67 + 3.07L_n + 1.66w + 2.53v - 0.7725L_n \cdot v + 0.7825w \cdot v + 1.4L_n^2 \quad (1)$$

where, PC is the power consumption, kW; L_n is the vertical distance of the rear shaft relative to the front shaft, mm; w is the rotational speed of the blade shaft, r/min; and v is the machine's forwards speed, m/s.

Design Expert software was used to obtain the normal probability distribution of the power consumption residuals, the distribution of the residuals versus the predicted values, and the distribution of the predicted values versus the actual values (Figure 7). The distribution points of the power consumption residuals versus the predicted values are scattered, whereas the points of the predicted values and actual values are distributed near the same straight line as the points of the power consumption

residual normal probability.

The three response surface graphs in Figure 8 reveal that as the depth of rotary tillage increases, the power consumption of the blade shaft gradually tends to increase. This occurred because with increasing tillage depth, more soil particles obstruct the movement of the rotary tiller blade, and the cohesive force between the soil particles in the plow pan is greater than that in the tillage layer. As the forwards speed and rotational speed of the blade shaft increase, the power consumption of the blade shaft also tends to gradually increase, but the rate of increase is relatively small. An interaction occurs between L_n and v and between w and v. Therefore, in actual rotary tillage operations, to ensure the tillage depth and straw burial rate, it is advisable to choose smaller values for the blade shaft rotational speed and the tillage depth of the front blade shaft while selecting a higher forwards speed to improve the operational efficiency and reduce power consumption per unit area.

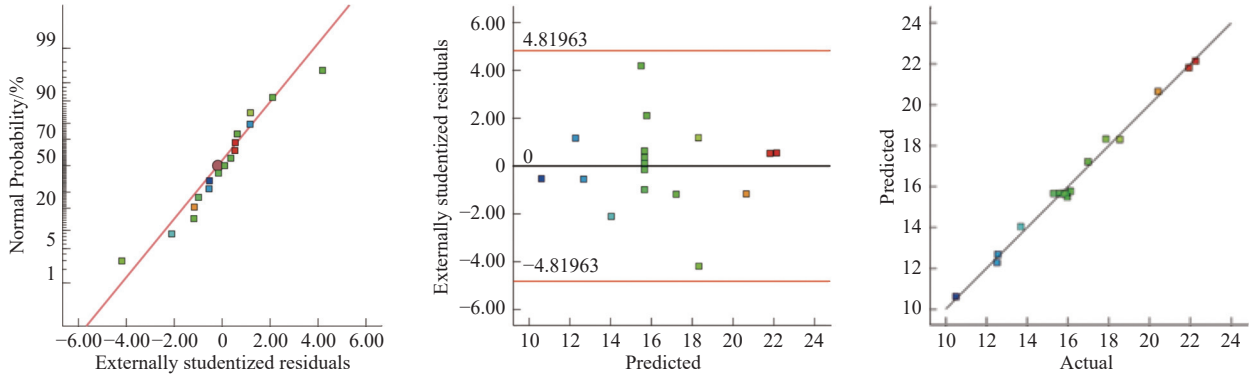

a. Normal probability distribution of power consumption residuals

b. Distribution of residuals versus predicted values

c. Distribution of predicted values versus actual values

Figure 7 Power consumption response surface model

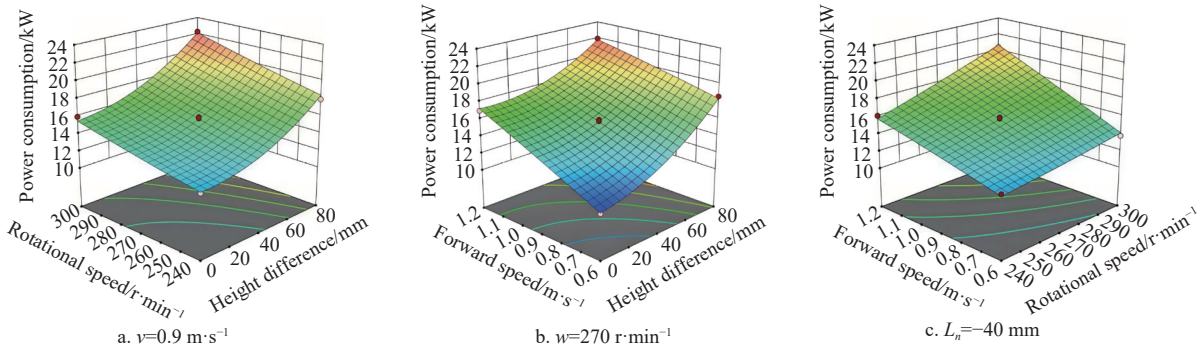

a. v=0.9 m·s^{-1}

b. w=270 r·min^{-1}

c. L_n=−40 mm

Note: L_n is the vertical distance of the rear shaft relative to the front shaft (mm), w is the rotational speed of the blade shaft (r·min^{-1}), and v is the machine's forwards speed (m·s^{-1}).

Figure 8 Influence of L_n, w, v on power consumption

4.2.2 Response surface analysis for the straw burial rate

The influence of the tillage parameters on the straw burial rate in the biaxial rotary tillage simulation tests is listed in Table 8. Multiple regression fitting was conducted on the simulation test results, with the ANOVA results in Table 9. The F-value of the quadratic model for the straw burial rate response surface is 1535.16 (p<0.0001), indicating that the fitting model is highly significant. The lack-of-fit term has p>0.05, suggesting that the lack of fit is not significant. This finding implies that the quadratic model for the straw burial rate response surface has a good fit with minimal error interference. The ANOVA results show that for the straw burial rate index, the regression terms L_n, w, v, $L_n \cdot w$, $w \cdot v$, L_n^2, and w^2 have highly significant impacts.

Insignificant terms were removed from the model, retaining the coefficients of significant terms. The regression equation for the straw burial rate M was refitted, ensuring a highly significant fit. The optimized regression equation is as follows:

$$M = 91.92 + 2.17L_n + 0.9638w - 445v + 0.35L_n \cdot w - 0.3025L_n \cdot v + 0.3775w \cdot v + 1.04L_n^2 - 0.4645w^2 + 0.023v^2 \quad (2)$$

where, M is the straw burial rate, %.

Table 8 Influence of tillage parameters on the straw burial rate in the biaxial deep rotary tillage simulation

Serial number	L_n/mm	w/r·min^{-1}	v/m·s^{-1}	M/%
1	0	0	0	91.88
2	−1	0	−1	90.94
3	1	0	1	94.42
4	0	−1	1	89.72
5	−1	1	0	90.97
6	0	−1	−1	91.32
7	1	1	0	95.95
8	0	1	−1	92.49
9	0	1	1	92.40
10	0	0	0	91.97
11	1	0	−1	95.96
12	−1	−1	0	89.74
13	−1	0	1	90.61
14	0	0	0	91.99
15	1	−1	0	93.32

Note: M is straw burial rate, %.

Table 9 Variance analysis results of straw burial rate response surface model

Source	Quadratic sum	Freedom	Mean square	*F*-value	*p*-value
Model	53.48	9	5.94	1535.16	< 0.0001**
L_n	37.80	1	37.80	9766.03	< 0.0001**
w	7.43	1	7.43	1919.67	< 0.0001**
v	1.58	1	1.58	409.28	<0.0001**
$L_n \cdot w$	0.49	1	0.49	126.59	<0.0001**
$L_n \cdot v$	0.366		0.366	94.56	<0.0001**
$w \cdot v$	0.57	1	0.57	147.27	<0.0001**
L_n^2	4.51	1	4.51	1166.39	< 0.0001**
w^2	0.9085		0.9085	234.70	<0.0001**
v^2	0.0022		0.0022	0.5754	0.4729
Residual error	0.0271	7	0.0039		
Lack of fit	0.0132	3	0.0044	1.26	0.3996
Pure error	0.0139	4	0.0035		
Summation	53.51	16			

** indicates highly significant (p<0.01).

Figure 9 shows the residual normal probability distribution, the distribution of residuals versus the predicted values, and the distribution of the predicted versus actual values for the straw burial rate. The results indicate that the residuals for the straw burial rate are dispersed relative to the predicted values, and both the residual normal probability points and the points for the predicted versus actual values cluster closely along a single line.

Figure 10 presents the response surface results for the influence of tillage parameters on the straw burial rate. The straw burial rate initially increases and then decreases with increasing rotational speed of the blade shaft (Figure 10a) and increases with greater front shaft tillage depth (Figure 10b). The straw burial rate also tends to first increase but then decrease with increasing blade shaft forwards speed and rotational speed (Figure 10c).

4.2.3 Optimal parameter response surface prediction analysis

The objective of parameter optimization in this section is to identify a set of tillage parameters that achieve a high straw burial rate and low power consumption while ensuring the quality of tillage operations. This is done using regression equations and the objective function method. The objective function for parameter optimization is as follows:

$$\begin{cases} P_n(L_n, w, v) \rightarrow \min \\ M(L_n, w, v) \rightarrow \max \end{cases} \tag{3}$$

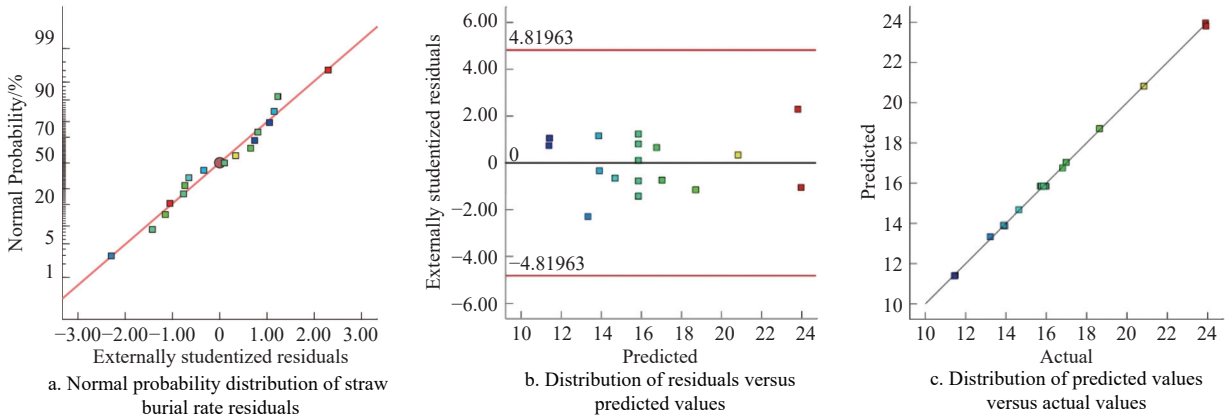

a. Normal probability distribution of straw burial rate residuals
b. Distribution of residuals versus predicted values
c. Distribution of predicted values versus actual values

Figure 9 Straw burial rate response surface model

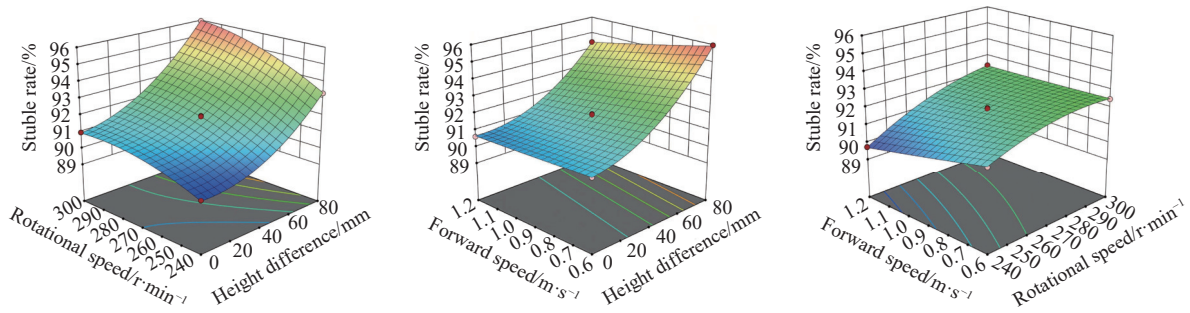

a. v=0.9 m·s^{-1}
b. w=270 r·min^{-1}
c. L_n=−40 mm

Note: L_n is the vertical distance of the rear shaft relative to the front shaft, mm; w is the rotational speed of the blade shaft, r/min; and v is the machine's forwards speed, m/s.

Figure 10 Influence of L_n, w, v on straw burial rate

The preprocessing settings for optimal parameter analysis are outlined in Table 10. Given the importance of straw return, the importance of the straw burial rate was assigned a weight of 5, whereas power consumption was given a weight of 3. The optimal parameters determined using Design-Expert software are a vertical distance of –73.3 mm between the rear and front shafts, a rotational speed of 273.6 r·min^{-1} for the front and rear rotary blades, and a forward speed of 0.6 m/s for the blades. Correspondingly, the

Table 10 Pretreatment settings for optimal parameter analysis

Object	Target	Lower limit	Upper limit	Weight	Importance
L_n	Range in	0	80	1	3
w	Range in	240	300	1	3
v	Range in	0.6	1.2	1	3
PC	Minimum value	10.5	22.6	1	3
M	Maximum value	89.72	95.96	1	5

predicted performance indicators are a power consumption of 17.4 kW and a straw burial rate of 95.3%. The optimal parameter combination set obtained from simulation analysis can serve as a reference basis for the design and manufacturing of physical prototype.

5 Field trials

5.1 Overview of the test area

The performance tests for the device were conducted in a typical double-cropping rice-wheat rotation region, located in Jiangyan District, Taizhou city, Jiangsu Province (120°07 ′E, 32°36 ′N). This area is the same as the soil sampling zone from which particles for model construction were obtained. The soil texture in the top 30 cm profile was classified as silty clay loam, according to the USDA classification, with mass fractions of sand, silt, and clay of 27.3%, 42.3%, and 30.4%, respectively. Table 11 lists the basic physical properties of the soil in the test area.

Table 11 Soil physical and chemical properties of test area

Soil characteristics	Value
Sand (0.05-2.00 mm)/%	27.3
Silt (0.002-0.050 mm)/%	42.3
Clay (<0.002 mm)/%	30.4
Soil bulk density/g·cm^{-3}	1.59
Volumetric water content/%	23.1
Soil compaction/MPa	2.17
Organic matter/g·kg^{-1}	19.3

5.2 Test equipment and procedure

The prototype of the designed biaxial rotary tillage device and its field test setup are shown in Figure 11. The device mainly consists of rotary tillage and power transmission components. The rotary tillage components include front and rear rotary blade groups, which are arranged in front-back and up-down configurations. The horizontal distance between the front and rear rotary blade groups is 45-50 cm, and the vertical height difference is 7.5 cm. The working power of the prototype is transmitted from the tractor through a universal joint to the intermediate gearbox, which then reduces the speed and increases the torque before the power is distributed to the rotary blade groups through a transmission cross shaft. The main technical parameters of the prototype are shown in Table 12.

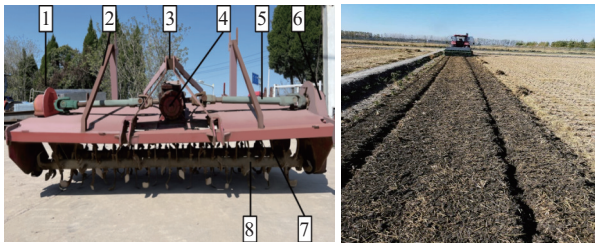

1. Siderear transmission gearbox 2. frame 3. Three-point suspension device 4. Intermediate transmission gear box 5. Transmission shaft 6.side front transmission gearbox 7. backward rotary blade group 8. forward rotary blade group

Figure 11 Biaxial rotary tillage prototype and field experiment scene

The test area follows a long-term rice-wheat double-cropping system. In accordance with local agronomic practices, rice is typically harvested in mid-October. During mechanical harvesting, the rice stubble height is less than 15 cm, and all the straw is crushed and scattered on the surface by the harvester. Field experiments on tillage quality were conducted after rice harvest (late October). A commonly used rotary tiller (1GQQN rotary tiller, China YTO Group Corporation) in the test plot was selected as a control (CK) to compare the tillage quality of the prototype (DT). Each tillage test was repeated three times, with each run covering no less than 50 m.

Table 12 Main technical parameters of biaxial rotary tillage

Serial No.	Parameters	Value	Unit
1	Size (length×width×height)	3200×2650×1200	mm
2	Power	88.2	kW
3	Rotary tillage depth	200-220	mm
4	Working width	2650	mm
5	Transmission mode	Side drive	
6	Rotary blade roller speed	200-280	r·min^{-1}

5.3 Testing indicators and methods

The performance testing indicators and methods for rotary tillage were obtained from the national standard of the People's Republic of China, GB/T 5668-2017 Rotary Tiller Standard. The soil bulk density before and after tillage, straw burial rate, surface flatness after tillage, and tillage depth stability were analyzed. The soil bulk density was determined by ring knife sampling and drying methods. The straw burial rate was measured using the five-point method, where five 1 m×1 m sampling points in the tillage area were selected, and the straw masses on the surface before and after tillage were compared. After the rotary tillage operation, tillage depth was measured using a vertical steel ruler, with 20 measurements taken per run, spaced approximately 2 m apart in the forward direction. To measure surface flatness after tillage, a horizontal reference line was drawn perpendicular to the forward direction of the machine, and multiple sampling points were selected to measure the vertical distance based on the horizontal reference line. The calculation of surface flatness after tillage is as follows:

$$K_j = \sqrt{\frac{\sum_{i=1}^{n_j}(b_{ji}-b_j)^2}{n_j-1}},\quad K = \frac{\sum_{j=1}^{N}K_j}{N} \tag{4}$$

where, K_j is the standard deviation of the vertical distance of each point from the horizontal reference line in the j-th run, cm; b_j is the mean vertical distance of each point from the horizontal reference line in the j-th run, cm; b_{ji} is the vertical distance of the i-th point from the horizontal reference line in the j-th run, cm; n_j is the number of measurement points in the j-th traverse; N is the total number of traverses measured, and K is the surface flatness after tillage.

5.4 Statistical methods

Statistical analysis was performed using SPSS software. The average value of each measurement was calculated, and multiple comparisons were made between different treatments, with treatment effects evaluated based on the least significant difference method. Graphs were drawn using Origin 9.0.

5.5 Results and analysis

The bulk density of each soil layer under the different tillage treatments is shown in Figure 12. In general, within the 30 cm soil layer, the soil bulk density gradually increased with depth. The mean bulk densities under the CK and DT treatments increased from 1285 and 1257 kg/m^3 to 1475 and 1383 kg/m^3, respectively. Moreover, in the 0-10 cm, 10-20 cm, and 20-30 cm soil layers, the DT treatment resulted in a reduction in the soil bulk density by

2.11%, 3.95% (p=0.05), and 6.20% (p=0.05), respectively, compared with traditional rotary tillage equipment (CK).

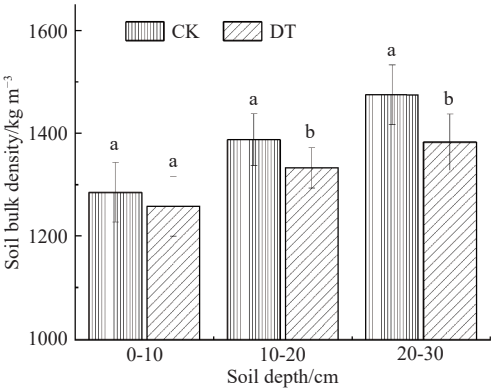

Note: Mean values within the same soil depth followed by a different letter are significantly different (p=0.05).

Figure 12 Mean soil bulk density to the depth of 30 cm for traditional single-axis rotary tillage equipment (CK), and biaxial rotary tillage equipment (DT) treatments

The quality of straw returned to the field using the two types of equipment is listed in Table 13. Overall, the tested equipment both met the national standards (GB/T 5668-2017) and Jiangsu provincial local standards (DB32/ 3688-2019) regarding straw burial rate, surface flatness, tillage depth, and stability. However, advantages were observed in all indicators for the DT treatment. Specifically, compared with the CK treatment, the DT treatment resulted in an increase in tillage depth of 80.23% (p=0.05), straw burial rate by 4.34% (p=0.05), and soil surface flatness of 13.04% (p=0.05).

Table 13 Field tillage test results

Treatment	Straw burial rate/%	Rotary tillage depth/mm	Depth stability/%	Surface flatness/mm
CK	85.41±1.73 b	114.8 ± 11.9 b	89.6	3.22 b
DT	92.60±1.22 a	206.9 ± 9.70 a	95.3	2.80 a
Standards *	≥80	≥80	≥85	≤5

Note: CK is traditional single-axis rotary tillage; DT is biaxial rotary tillage. Different letters following the same column of data indicate a significant difference at p= 0.05. * The national and local standards are GB/T 5668-2017 Rotary Tiller Standard and DB32/3688-2019 Jiangsu Provincial Local Standard.

6 Conclusions

This study was situated within the agronomic policy background of total rice straw returning in the rice-wheat rotation system of the mid-lower region of the Yangtze River in China. In this context, we established a stubble-soil-straw discrete element composite model using the DEM and coupled it with a biaxial layered cutting rotary tillage system. Through response surface methodology, the optimal parameter combination for the vertical height difference of the blade shaft relative to the front blade shaft (L_n), blade group rotational speed (w), and machine forwards speed (v) was determined to be L_n = –73.3 mm, w = 273.6 r/min, and v = 0.6 m/s. The field test results demonstrated that the prototype achieved a tillage depth of 206.9 mm, a tillage depth stability of 95.3%, a soil surface evenness of 2.80 cm, and a straw burial rate of 92.6%, all of which met the quality requirements for rotary straw tillage. Given the advantages of straw return in improving soil conditions and promoting crop growth, these findings provide a theoretical basis and practical case reference for achieving high-quality mechanized straw return in rice-wheat rotation systems.

Overall, this study still presents the following limitations: 1) Due to the substantial computational demands of the coupled simulation model, the fragmentation mechanisms of straw and stubble were not considered; 2) The agronomic effectiveness of this technical solution requires further validation through cultivation practices. In the follow-up study, the long-term effects of biaxial deep rotary tillage on soil physical properties (such as porosity, permeability, etc.), soil microbial community structure, and crop growth will be further studied to thoroughly evaluate the comprehensive benefits. It also needs to address the compatible operation of biaxial rotary tillage device with other agricultural machinery to provide a more reliable technical solution for efficient land preparation and high-quality seedbed environments.

Acknowledgements

This work was financially supported by National Key Research and Development Program of China (Grant No. 2024YFD2000203) and the Jiangsu Provincial Modern Agricultural Machinery and Equipment Technology Demonstration and Extension Project (Grant No. NJ2023-03).

[References]

[1] Li H, Dai M W, Dai S L, Dong X J. Current status and environment impact of direct straw return in China's cropland-A review. Ecotoxicology and Environmental Safety, 2018; 159: 293–300.

[2] Huo R X. Long-term straw return enhanced crop yield by improving ecosystem multifunctionality and soil quality under triple rotation system: An evidence from a 15 years study. Field Crops Research, 2024; 312: 109395.

[3] Li P, Yin W, Fan Z L, Hu F L, Zhao L H, Fan H, et al. Improving crop productivity by optimizing straw returning patterns to delay senescence of wheat leaves. European Journal of Agronomy, 2024; 159: 127274.

[4] Chen H, Elahi E, Lei X Y. Impact of different straw treatment methods on agricultural production efficiency: An empirical evidence of Jiangsu Province of China. Frontiers in Environmental Science, 2022; 10: 986921.

[5] Cheng Z, Li A J, Wang R G, Hu Q, Zhou J, Li M, et al. Long-term straw return promotes accumulation of stable soil dissolved organic matter by driving molecular-level activity and diversity. Agriculture, Ecosystems & Environment, 2024; 374: 109155. DOI: 10.1016/j.agee.2024.109155.

[6] Liu Q, Dai H C, Wang L, Qian X, Gao Y B, Zhang H, et al. Microbial community and functions depending on tillage and straw returning management: Consequences for soil health and ecosystem services. Land Degradation & Development, 2024; 35(17): 5357–5366.

[7] Han J X, Song X Y, Fu H Y, Liu C G, Yang F S. Effects of the decomposition agent application on the physicochemical properties and microbial community structure of wheat straw-returning soil. Environmental Technology & Innovation, 2024; 35: 103668.

[8] Liu F Y, Gao M L, Zhang H Z, Yuan H B, Hu B, Zong R, et al. Synergistic impact of various straw-return methods and irrigation regimes on winter wheat physiological growth and yield. Field Crops Research, 2024; 316: 109516.

[9] Chen K W, Ma T, Ding J H, Yu S E, Dai Y, He P R, et al. Effects of Straw Return with Nitrogen Fertilizer Reduction on Rice (Oryza sativa L.) Morphology, Photosynthetic Capacity, Yield and Water-Nitrogen Use Efficiency Traits under Different Water Regimes. Agronomy-Basel, 2023; 13(1): 133.

[10] Bao X B, Zhao X Y, He J, Li H W, Wang Q J, Liu W Z. Design and performance test of plowing and rotary tillage combined machine. Inmateh-Agricultural Engineering, 2019; 58(2): 213–222.

[11] Liu D J, Hu J L, Gong Y, Chen X, Wang G, Zhang X, et al. Design and experiment of suspended rotary tillage ridge and film mulching machine. Inmateh-Agricultural Engineering, 2023; 69(1): 237–244.

[12] Matin M A, Fielke J M, Desbiolles J M A. Furrow parameters in rotary strip-tillage: Effect of blade geometry and rotary speed. Biosystems Engineering, 2014; 118: 7–15.

[13] Yang W, Xiao X, Pan R H, Guo S Y, Yang J. Numerical Simulation of Spiral Cutter-Soil Interaction in Deep Vertical Rotary Tillage. Agriculture-Basel, 2023; 13(9): 1850.

[14] Zheng K, Cheng J, Xia J F, Liu G Y, Xu L. Effects of Soil Bulk Density and Moisture Content on the Physico-Mechanical Properties of Paddy Soil in Plough Layer. Water, 2021; 13(16): 2290.
[15] Xiao W S, Niu P, Wang P, Xie Y J, Xia F. Simulation analysis and optimization of soil cutting of rotary blade by ansys/ls-dyna. Inmateh-Agricultural Engineering, 2024; 72(1): 22–32.
[16] Zhang X Y, Hu X, Zhang L X, Kheiry A N O. Simulation and structural parameter optimization of rotary blade cutting soil based on SPH method. Int J Agric & Biol Eng, 2024; 17(3): 82–90.
[17] Shi Y Y, Wang X C, Hu Z C, Gu F W, Wu F, Chen Y Q. Optimization and experiment on key structural parameters of no-tillage planter with straw-smashing and strip-mulching. Int J Agric & Biol Eng, 2021; 14(3): 103–111.
[18] Yuan Y W, Wang J Y, Zhang X, Zhao S H. Study on tillage resistance and energy consumption of a plain straight rotary blade for strip tillage. Engenharia Agricola, 2023; 43(2): e20220127.
[19] Xiao M H, Ma Y, Wang C, Chen J Y, Zhu Y J, Bartos P, et al. Design and experiment of fuzzy-PID based tillage depth control system for a self-propelled electric tiller. Int J Agric & Biol Eng, 2023; 16(4): 116–125.
[20] Liu G Y, Zheng K, Xia J F, Cheng J, Liu Z Y, Wei Y S, et al. Research on an intelligent vibration detachment system for rotary tiller based on soil surface roughness dynamic characteristics. Computers and Electronics in Agriculture, 2024; 224: 109214.
[21] Du J, Heng Y F, Zheng K, Zhang W L, Zhang J M, Xia J F. Evaluation of the Performance of a Combined Tillage Implement with Plough and Rotary Tiller by Experiment and DEM Simulation. Processes, 2021; 9(7): 1174.
[22] Zheng K, McHugh A D, Li H W, Wang Q J, Lu C Y, Hu H N, et al. Design and experiment of anti-vibrating and anti-wrapping rotary components for subsoiler cum rotary tiller. Int J Agric & Biol Eng, 2019; 12(4): 47–55.
[23] Coetzee C J. Calibration of the discrete element method. Powder Technology, 2017; 310: 104–142.
[24] Yan D X, Yu J Q, Wang Y, Zhou L, Sun K, Tian Y. A Review of the Application of Discrete Element Method in Agricultural Engineering: A Case Study of Soybean. Processes, 2022; 10(7): 1305.
[25] Mak J, Chen Y, Sadek M A. Determining parameters of a discrete element model for soil-tool interaction. Soil & Tillage Research, 2012; 118: 117–122.
[26] Walton O R, Braun R L. Stress calculations for assemblies of inelastic speres in uniform shear. Acta Mechanica, 1986; 63(1): 73–86.
[27] Ucgul M, Fielke J M, Saunders C. Three-dimensional discrete element modelling (DEM) of tillage: Accounting for soil cohesion and adhesion. Biosystems Engineering, 2015; 129: 298–306.
[28] Zhang X Y, Yu S Y, Hu X, Zhang L X. Study on rotary tillage cutting simulations and energy consumption predictions of sandy ground soil in a Xinjiang cotton field. Computers and Electronics in Agriculture, 2024; 217: 108646.
[29] Chen G B, Wang Q J, Li H W, He J, Wang X H, Zhang X Y, et al. Experimental research on vertical straw cleaning and soil tillage device based on Soil-Straw composite model. Computers and Electronics in Agriculture, 2024; 216: 108510.
[30] Wang J W, Xu Y A, Wang C Y, Xiang Y S, Tang H. Design and simulation of a trenching device for rice straw burial and trenching based on MBD-DEM. Computers and Electronics in Agriculture, 2023; 207: 107722.
[31] Lin J X, Liao Q X, Wang X F, Kang Y, Du W B, Zhang Q S. Exploring straw movement through the simulation of shovel-type seedbed preparation machine-straw-soil interaction using the DEM-MBD coupling method. Computers and Electronics in Agriculture, 2024; 226: 109465.
[32] Zhu D Q, Shi M H, Yu C Y, Yu Z Y, Kuang F M, Xiong W, et al. Tool-straw-paddy soil coupling model of mechanical rotary-tillage process based on DEM-FEM. Computers and Electronics in Agriculture, 2023; 215: 108410.
[33] Zhang J, Xia M, Chen W, Yuan D, Wu C Y, Zhu J P. Simulation Analysis and Experiments for Blade-Soil-Straw Interaction under Deep Ploughing Based on the Discrete Element Method. Agriculture-Basel, 2023; 13(1): 136.
[34] Xu G M, Xie Y X, Joseph O A, Chen X X, Matin M A, Abbas A, et al. A novel method for measuring and evaluating spatial distribution of straw incorporated by rotary tillage. Agronomy Journal, 2022; 114(1): 853–866.
[35] Xu G M, Xie Y X, Matin M A, He R Y, Ding Q S. Effect of Straw Length, Stubble Height and Rotary Speed on Residue Incorporation by Rotary Tillage in Intensive Rice-Wheat Rotation System. Agriculture-Basel, 2022; 12(2): 222.
[36] Xu G M, Xie Y X, Liang L, Ding Q S, Xie H X, Wang J N. Straw-Soil-Rotary Blade Interaction: Interactive Effects of Multiple Operation Parameters on the Straw Movement. Agronomy-Basel, 2022; 12(4): 847.
[37] Miressa S B, Ding Q S, Li Y N, Amisi E O. Optimization of Tillage Operation Parameters to Enhance Straw Incorporation in Rice-Wheat Rotation Field. Agronomy-Basel, 2025; 15(1): 54.
[38] Liu C Z, Si B C, Zhao Y, Wu Z M, Lu X C, Chen X, et al. Drivers of soil quality and maize yield under long-term tillage and straw incorporation in Mollisols. Soil & Tillage Research, 2025; 246: 106360.
[39] Du J, Heng Y F, Zheng K, Luo C M, Zhu Y H, Zhang J M, et al. Investigation of the burial and mixing performance of a rotary tiller using discrete element method. Soil & Tillage Research, 2022; 220: 105349.
[40] Hu J P, Zhao J, Pan H R, Liu W, Zhao X S. Prediction model of double axis rotary power consumption based on discrete element method. Transactions of the CSAM, 2020; 51(S1): 9–16. (in Chinese)
[41] Xu C S, Xu F D, Tang H, Wang J W. Determination of Characteristics and Establishment of Discrete Element Model for Whole Rice Plant. Agronomy-Basel, 2023; 13(8): 2098.
[42] Lenaerts B, Aertsen T, Tijskens E, De Ketelaere B, Ramon H, De Baerdemaeker J, et al. Simulation of grain-straw separation by Discrete Element Modeling with bendable straw particles. Computers and Electronics in Agriculture, 2014; 101: 24–33.